BioMedInformatics

MDPI

Article

A Comparative Dual-Platform Docking and Dynamic Light Scattering Analysis of Nutraceutical Interactions with the ApoE4–oxLDL Complex

Giorgia Francesca Saraceno, Daniela Sorrenti, Claudia Ferraro and Erika Cione *

Department of Pharmacy, Health and Nutritional Sciences, University of Calabria, 87036 Rende, Italy; giorgiafrancesca.saraceno@unical.it (G.F.S.); srrdnl99p63m208x@studenti.unical.it (D.S.); claudia.ferraro@unical.it (C.F.)

* Correspondence: erika.cione@unical.it

Abstract

Background: Targeting Apolipoprotein E4 (ApoE4) represents a frontier in Alzheimer's disease therapeutics. This study investigates the therapeutic potential of a nutraceutical panel (Polydatin, trans-resveratrol, luteolin, and PEA) by exploring their interaction with the ApoE4 EZ-482 cavity. Methods: Using a dual-platform docking strategy (SwissDock and Schrödinger Maestro) across three structural constructs. Results and Discussion: We identified the full-length protein (1–299) as the optimal target, showing a robust correlation between normalized docking scores (Spearman $\varrho = 0.79$). Crucially, biophysical analysis via dynamic light scattering (DLS) revealed that the ApoE4–oxLDL complex exhibits a ζ-potential of -10.97 mV, a state prone to pathological aggregation. Luteolin and PEA effectively altered this electrostatic environment, inducing significant positive shifts to +2.15 mV and +1.05 mV, respectively. The alignment between computational rankings and experimental ζ-potential perturbations supports the predictive reliability of our model. These findings suggest that nutraceuticals can modulate the ApoE4–oxLDL biophysical profile and highlight that a full structural context is mandatory for developing effective ApoE4-targeted interventions.

Keywords: apolipoprotein E4; nutraceuticals; molecular docking; ζ-potential; luteolin; oxLDL; dynamic light scattering; structure-based drug design; protein–lipid interactions

1. Introduction

Apolipoprotein E4 (ApoE4) plays a central role in lipid metabolism within the central nervous system and is widely recognized as the strongest genetic risk factor for Alzheimer's disease (AD) in Italy and worldwide [1,2]. Extensive evidence from human studies and transgenic animal models indicates that ApoE isoforms differentially influence cerebral amyloid burden and disease progression [3,4]. These isoform-specific effects are increasingly attributed to distinct conformational and surface properties that modulate interactions with amyloid-β (Aβ) [5–7]. Despite the isoforms diverging by only one amino acid substitution, ApoE4 displays distinct structural and functional characteristics that translate into disproportionately large structural and functional consequences in AD. ApoE isoforms exert markedly distinct effects on Aβ aggregation, clearance and neurotoxicity following the well-established hierarchy ApoE4 > ApoE3 > ApoE2 [8–10]. Therefore, of the three major human isoforms, ApoE4 is uniquely associated with increased Aβ deposition, reduced clearance efficiency, and heightened susceptibility to neurodegeneration [11,12], as also

Academic Editor: Hans Binder

Received: 19 March 2026
Revised: 6 May 2026
Accepted: 13 May 2026
Published: 15 May 2026

by structure-based studies [13,14]. The modulation of ApoE4 structure and function by small molecules has attracted increasing attention as a potential therapeutic strategy [15]. Within this context, EZ-482 represents the most extensively characterized small molecule interacting with the ApoE C-terminal domain [16]. Experimental investigations combining biophysical techniques with hydrogen/deuterium exchange mass spectrometry (HDX-MS) have demonstrated that EZ-482 binds discrete regions of the C-terminal domain in both ApoE3 and ApoE4 but selectively induces allosteric conformational changes in the N-terminal domain of ApoE4 upon binding, illustrating subtle variations in ligand–protein interaction geometry [16]. Of note, the C-terminal domain recognizes lipoproteins. Oxidized low-density lipoprotein (oxLDL) could interact with ApoE4 [17,18]. Within this framework, modulation of ApoE itself rather than direct targeting of Aβ has emerged as a promising therapeutic strategy for cognitive decline [19,20]. Early cognitive decline may be counteracted by micronutrients [21,22] or by bioactive molecules known as nutraceuticals. Nutraceuticals such as polydatin, trans-resveratrol, luteolin, and palmitoylethanolamide (PEA) display neuroprotective properties at different levels. Their potential role has been increasingly explored in modulating AD-related pathways [23–26]. Their capability to interact with ApoE4 is relatively unknown. Here, to understand their potential activity, an ApoE4 dual-platform docking strategy was employed using SwissDock (Attracting Cavities algorithm) and Schrödinger Maestro Glide (grid-based docking) to reduce platform-specific bias. Anchoring biocomputational analyses to experimental data is essential to enhance both the interpretability and translational relevance of in silico predictions. Therefore, dynamic light scattering (DLS) measurements were performed to determine nutraceutical-induced changes in the ζ-potential of the ApoE4–oxLDL system.

2. Materials and Methods

2.1. Protein Structure Preparation and Ligand SMILES

The three-dimensional structure of human ApoE3 was retrieved from the Protein Data Bank (PDB ID: 2L7B) and used as the reference structure. The ApoE4 isoform was generated in silico from the ApoE3 structure by introducing the Cys112 → Arg substitution. Truncated constructs corresponding to the C-terminal domain (residues 216–299) and to the HDX-MS-identified segment (residues 229–265) were also generated. For SwissDock calculations, protein preparation was handled automatically by the SwissDock server, which internally assigns protonation states and performs ligand and receptor preparation as part of the EADock DSS docking workflow. For Schrödinger-based docking calculations, protein structures were prepared using the Protein Preparation Wizard implemented in Schrödinger Maestro. Hydrogen atoms were added, bond orders were assigned, and protonation states were generated at physiological pH. The structures were subsequently subjected to restrained energy minimization using the OPLS force field to remove steric clashes while preserving the overall fold. The structural quality of the human ApoE3 model (PDB ID: 2L7B) and the derived ApoE4 isoform was evaluated using the Protein Structure Analysis (ProSA) web server [27]. ProSA assesses structural reliability by comparing the overall energy profile of a model with experimentally determined protein structures obtained from X-ray crystallography and nuclear magnetic resonance (NMR) studies. The corresponding ProSA validation analysis and Z-score for ApoE3 are provided in the Supplementary Materials (Figure S1). Ligand structures were obtained as SMILES strings from public chemical databases or the literature sources, as reported below:

- EZ-482: O=C(NC1=CC(=CC=C1O)S(=O)(=O)NC=2C=CC=C(Cl)C2)CC3=NN(C(=O)C=4C=CC=CC43).
- Polydatin: C1=CC(=CC=C1C=CC2=CC(=CC(=C2)OC3C(C(C(C(O3)CO)O)O)O)O)O.
- Trans-resveratrol: C1=CC(=CC=C1C=CC2=CC(=CC(=C2)O)O)O.

- Luteolin:C1=CC(=C(C=C1C2=CC(=O)C3=C(C=C(C=C3O2)O)O)O)O.
- PEA: CCCCCCCCCCCCCCCC(=O)NCCO.

2.2. Molecular Docking Using SwissDock and Schrödinger Maestro Glide

Site-directed docking calculations were performed using SwissDock, a web-based docking platform based on the EADock DSS algorithm [28]. SwissDock performs a global exploration of ligand binding modes and ranks solutions using a physics-based scoring function derived from the CHARMM force field [29]. Docking solutions were clustered and ranked according to the estimated free energy of binding provided by SwissDock, and representative poses from the most favorable clusters were selected for comparison. For SwissDock simulations, ligands were provided either as SMILES strings or as mol2 structure files and ligand preparation was performed internally by the SwissDock server [28]. In parallel, docking calculations were performed using the Glide docking engine implemented in Schrödinger Maestro (Schrödinger LLC). Glide combines systematic sampling of ligand conformations within a predefined receptor grid with an empirical scoring function optimized for protein–ligand recognition [29–31]. Docking was carried out using the standard precision (SP) mode with default parameters. Binding poses were ranked according to the GlideScore scoring function, and the top-ranked conformation within the predefined binding site was selected for subsequent analysis. For Schrödinger-based docking, ligands were prepared using LigPrep with ionization and tautomeric states generated using Epik at pH 7.0 $\pm$ 0.2 and stereoisomers generated (LigPrep, Schrödinger, LLC, New York, NY, USA, 2025). For each ligand, the structure associated with the lowest state penalty was selected, and final geometries were energy-minimized using the OPLS force field [32] as described in the literature [33]. Consensus strategies are widely recognized to improve the reliability of virtual screening by averaging ranks across disparate scoring functions, thereby reducing false positives and system-bias effects, such as parameter overfitting or platform-dependent scoring dependence. Consistent with this, ligand poses were ranked by consensus, and all scores were normalized relative to the EZ-482 reference ligand to ensure internal methodological consistency [34,35]. A comparative overview of the two docking platforms is summarized in Table S1.

2.3. Analysis of Docking Score Normalization Strategy

Docking results obtained from SwissDock and Schrödinger Maestro Glide were analyzed independently and compared at the level of predicted binding geometries and residue-level interaction patterns within the predefined binding site. Given the methodological differences between the two docking platforms, absolute docking scores were not directly compared. Instead, qualitative consistency of ligand positioning and interacting residues was used as the primary criterion for cross-platform comparison, as recommended for multi-engine docking studies. Furthermore, docking scores were normalized relative to the EZ-482 ApoE reference ligand to facilitate internal comparison across ligands and ApoE isoforms. Normalization was performed using the following expression:

$$\Delta\Delta G = \Delta G_{lig} - \Delta G_{EZ\text{-}482}$$

where both ΔG values were obtained using the same docking platform and identical computational settings. Because docking scoring functions are platform dependent and do not represent absolute thermodynamic binding free energies, normalization relative to EZ-482 was adopted to enable comparison of relative binding trends while preserving internal consistency within each scoring framework.

2.4. Residue-Level Concordance Analysis of SwissDock and Schrödinger Maestro

To assess the consistency of predicted ligand residue interactions between SwissDock and Schrödinger Maestro Glide, residue-level concordance was quantified using set-based similarity metrics. Because docking scores are sensitive to platform-specific scoring functions and sampling strategies, residue-level concordance was analyzed as a complementary measure to evaluate the structural consistency of predicted ligand–ApoE interactions. For each ligand, amino acid (a.a.) residues identified as interacting with the protein were extracted from both docking platforms. The Jaccard index was calculated as:

$$\text{Jaccard}\ (A, B) = |A \cap B| \div |A \cup B|$$

where A and B represent the sets of interacting residues identified by SwissDock and Schrödinger Maestro, respectively. A Jaccard value of 0 indicates no overlap, while a value of 1 indicates complete concordance between the two platforms. Additionally, the Sørensen–Dice coefficient was computed to account for differences in the size of the residue sets, as follows:

$$\text{Sørensen–Dice}\ (A, B) = 2|A \cap B| \div |A| + |B|$$

The Sørensen–Dice coefficient ranges from 0 to 1, with 0 indicating no overlap and 1 indicating complete similarity.

2.5. Preparation of Human ApoE4, oxLDL, and Nutraceuticals

Oxidized low-density lipoprotein (oxLDL, Catalog No. L34357), recombinant human ApoE4 (Catalog No. 350-04), and dimethyl sulfoxide (DMSO, Catalog No. A13280.36) were obtained from Thermo Fisher Scientific (Waltham, MA, USA). Polydatin (Catalog No. 15721), trans-resveratrol (Catalog No. PHR2201), luteolin (Catalog No. L9283) and bovine serum albumin (BSA, Catalog No. A7906) were purchased from Sigma-Aldrich (St. Louis, MO, USA). PEA (Catalog No. 504359) was obtained from Merck (Darmstadt, Germany). Dulbecco phosphate-buffered saline (DPBS) (Catalog No. AUL0615) was obtained from Aurogene (Rome, Italy). According to the certificate of analysis, the ApoE4 preparation requires the addition of BSA, which is included as a stabilizing protein to prevent self-aggregation of ApoE4. ApoE4 was diluted from a 1 mg/mL stock solution (1:1000 DPBS) and added to the final mixture to obtain a concentration of 37.3 ng/mL, while oxLDL was added from a 2.5 mg/mL stock solution to reach a final concentration of 2.5 µg/mL while maintaining a physiological ratio. The nutraceuticals were dissolved in DMSO and used at the doses of 50 ng/mL for polydatin and trans-resveratrol, 520 ng/mL for luteolin, and 28 ng/mL for PEA. The doses were set at approximately twofold the maximal plasma concentrations (Cmax) reported in the literature (see Table S2). The final DMSO concentration was 0.1% (*v*/*v*) in all samples, and the final volume was 1 mL in PBS. The ApoE4–oxLDL complex, with and without nutraceuticals, was incubated at 37 °C for 30 min.

2.6. Zeta-Potential Measurements by Dynamic Light Scattering

Zeta potential measurements were conducted using a Zetasizer Nano ZS instrument (Malvern Instruments, Worcestershire, UK) at 25 °C, employing disposable zeta potential cuvettes in accordance with the manufacturer's protocol. Each sample was analyzed under controlled conditions to ensure the reproducibility and accuracy of the electrophoretic mobility data, from which the zeta potential values were subsequently calculated by the instrument's integrated software.

To isolate the electrostatic contribution of the nutraceutical compounds, ζ-potential values were expressed relative to the ApoE4–oxLDL baseline, representing the electrostatic

properties of the system prior to ligand addition. All measurements were performed in triplicate.

3. Results and Discussion

3.1. Structural Validation of Human ApoE4 with the ProSA Web Server

The structural quality of the human ApoE model (PDB ID: 2L7B) and ApoE4 isoform was evaluated using ProSA [27]. The ApoE4 model yielded a Z-score of −3.35, indicating that the overall model energy falls within the range characteristic of native proteins of comparable size. The Z-score reflects global structural quality by quantifying the deviation of the total energy from an energy distribution derived from experimentally validated structures. Values outside the characteristic range typically indicate structural errors; in this case, the observed Z-score supports the structural suitability of the ApoE4 model for subsequent docking analyses (Figure 1).

3.2. Directed Docking on the HDX-MS EZ-482 Binding Cavity (229–265) C-Terminal (216–299) and ApoE4

Optimizing therapeutic molecules in drug discovery remains a complex challenge requiring innovative biocomputational approaches [36]. In this study, molecular docking simulations were initially performed using SwissDock with the Attracting Cavities algorithm [37], specifically targeting the EZ-482 binding cavity. This site, located within the ApoE4 C-terminal domain, exhibits a calculated dissociation constant Kd of 5–10 μM, corresponding to an estimated binding free energy ΔG of approximately −7.2 to −6.8 kcal/mol [16]. To ensure cross-platform validation and reduce software-specific bias, independent simulations were conducted using Schrödinger Maestro Glide with a grid-based site-directed protocol [38]. For the HDX-MS cavity (229–265), the grid was centered at x = −10.85, y = −0.88, z = 10.28 (30 × 30 × 30 Å). For the C-terminal domain (216–299), coordinates were x = −5.28, y = −0.05, z = 8.89 (30 × 30 × 30 Å), while for the full-length ApoE4 (1–299), the center was x = 0.37, y = 1.32, z = −0.24 (26.85 × 26.85 × 26.85 Å). Cross-platform agreement was quantified using Pearson (r) and Spearman (ϱ) correlations on docking scores normalized to EZ-482 (Table 1). For the HDX-MS cavity, correlation was low (r= −0.61; ϱ= −0.20) whereas the C-terminal (r= 0.55; ϱ = 0.71) and full-length ApoE4 (r = 0.74; ϱ = 0.79) showed progressively stronger alignment. These values reflect a robust prioritization of lead compounds consistently identified across independent docking frameworks, in line with consensus performance reported in the literature [35,39]. The same analyses for ApoE3 are reported in Table S3.

Table 1. Cross-platform correlation analysis of normalized docking scores (ΔΔG = ΔG_lig − ΔG_EZ-482) for HDX-MS EZ-482 binding cavity (229–265), truncated C-term (216–299) and ApoE4.

Region	Pearson	Spearman Rank	Interpretation
HDX-MS EZ-482 binding cavity (229–265)	−0.61	−0.2	Very low quantitative agreement; low ranking consistency
C-terminal (216–299)	0.55	0.71	Moderate quantitative agreement; moderate ranking consistency
ApoE4 (1–299)	0.74	0.79	Strong quantitative agreement; high ranking consistency

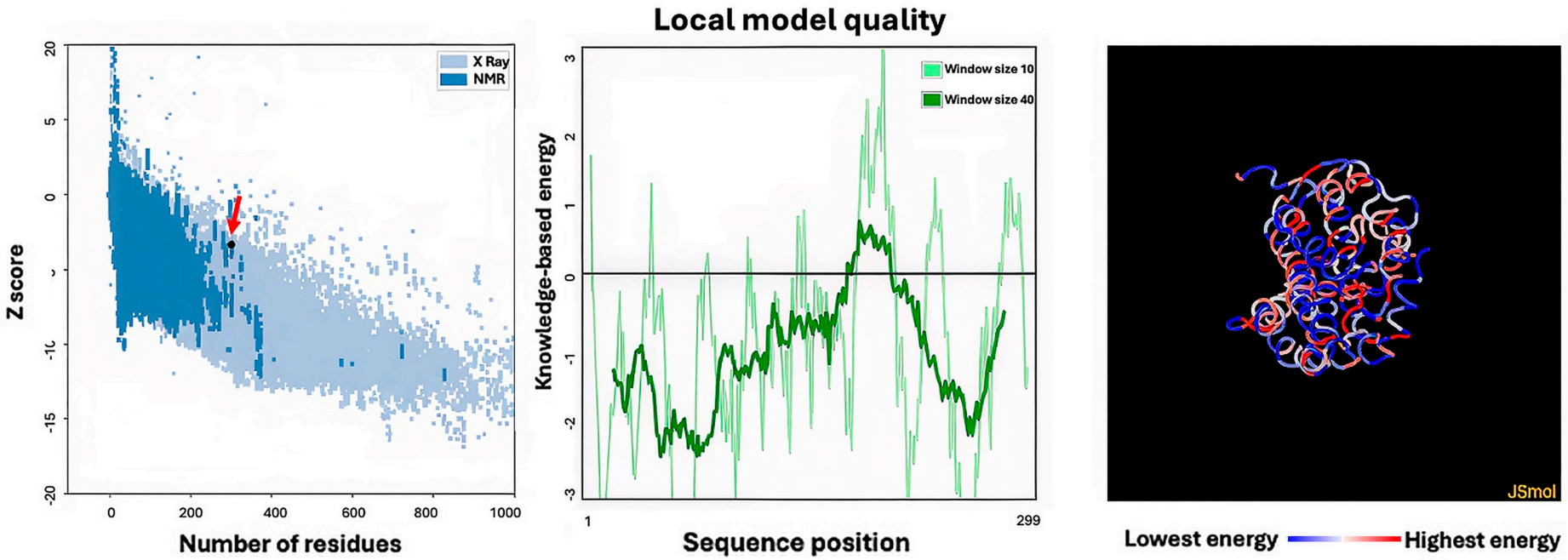

Figure 1. ProSA structural validation of the ApoE4. The (**left panel**) shows the Z-score of the ApoE4 structure relative to experimentally determined X-ray and NMR protein structures. The (**central panel**) reports residue-wise local model quality based on knowledge-based energy profiles. The (**right panel**) displays the three-dimensional structure colored according to local energy distribution from low (blue) to high (red).

Since the binding region was explicitly defined by prior biophysical characterization, these simulations aimed to evaluate ligand accommodation and relative energetics within a predefined microenvironment rather than identifying novel pockets [40]. The observed lack of concordance for the 229–265 segment suggests that this region does not function as an autonomous binding pocket when isolated from the broader structural context of the C-terminal domain.

3.3. Nutraceuticals Site-Directed Docking Assessment on ApoE4, C-Terminal (216–299) and HDX-MS EZ-482 Binding Cavity (229–265)

Docking scores were normalized relative to EZ-482 using the expression $\Delta\Delta G = \Delta G\_ligand - \Delta G\_EZ\text{-}482$ across the three structural constructs: the HDX-MS cavity (229–265), the C-terminal domain (216–299), and the full-length ApoE4 (1–299). The nutraceutical panel comprised polydatin, trans-resveratrol, luteolin, and PEA. SwissDock was employed as the primary docking platform, with subsequent replication using Schrödinger Maestro Glide to incorporate empirical scoring and force-field refinement. Utilizing docking-derived EZ-482 values as an internal anchor, rather than experimental free energies, ensures methodological coherence by avoiding the integration of fundamentally different energy definitions. This transformation yields a dimensionless, platform-specific metric that reflects relative deviations from the EZ-482 reference within a consistent scoring scale. Furthermore, this normalization provides an internal benchmark anchored to an experimentally characterized ligand, circumventing the direct comparison of docking scores with absolute thermodynamic values [31]. The same normalization procedure was applied to the corresponding ApoE3 simulations (Table S4), with all docking-derived energies summarized in Table 2.

Table 2. Docking-derived energies for nutraceutical compounds for HDX-MS EZ-482 binding cavity (229–265), truncated C-term (216–299) and ApoE4 (1–299) obtained by SwissDock and Schrödinger Maestro Glide.

Ligand	ΔΔ*G* SwissDock	ΔΔ*G* Schrödinger Maestro Glide
HDX-MS EZ-482 binding cavity (229–265)		
EZ-482	-	-
Polydatin	0.48	**−0.282**
Trans-resveratrol	1.10	0.113
Luteolin	0.80	0.069
PEA	0.35	5.497
C-terminal (216–299)		
Polydatin	0.89	**−1.24**
Trans-resveratrol	0.89	**−0.27**
Luteolin	0.68	**−0.61**
PEA	0.96	5.23
ApoE4 (1–299)		
Polydatin	1.21	**−0.30**
Trans-resveratrol	1.75	0.31
Luteolin	1.53	**−1.35**
PEA	1.95	3.93

In the Schrödinger Maestro Glide simulations, normalized values for the isolated HDX-MS cavity (229–265) were −0.282, 0.113, and 0.069 for polydatin, trans-resveratrol, and luteolin, respectively. For the truncated C-terminal domain (216–299), the corresponding values were −1.24, −0.27, and −0.61. Notably, in the full-length ApoE4 (1–299) construct, both polydatin and luteolin yielded negative values of −0.30 and −1.35, respectively. Within this docking framework, more negative normalized scores indicate a more favorable

predicted interaction relative to the EZ-482 reference. These results point to a potentially enhanced interaction propensity of luteolin when the full structural context of the protein is considered.

3.4. Residue-Level Concordance Analysis of HDX-MS EZ-482 Binding Cavity (229–265), C-Terminal (216–299) and Full-Length ApoE4 (1–299) and Shared Amino Acids

To quantify the similarity between the binding profiles of the nutraceuticals and the reference ligand EZ-482, both the Jaccard index and the Sørensen–Dice coefficient were calculated across the three structural constructs. Within the HDX-MS-defined binding cavity (229–265), similarity indices were zero for all compounds. In the C-terminal region (216–299), polydatin showed 12% similarity (Jaccard 0.12; Dice 0.21), while trans-resveratrol and luteolin exhibited minimal concordance (5% and 5.8%, respectively). Conversely, PEA showed a significantly higher overlap of 38%, suggesting a preferential accommodation within this hydrophobic C-terminal environment, which is known to facilitate association with lipophilic particles [38]. In contrast, the full-length ApoE4 (1–299) provided the highest overall concordance, consistent with the hypothesis that the entire protein structure is essential for the observed interaction geometry (Table 3). In this context, Polydatin achieved a 34% overlap (Jaccard 0.34; Dice 0.48), closely approximating the reference profile of EZ-482 (36% shared residues). Trans-resveratrol and luteolin showed intermediate concordance (27% and 23%), whereas PEA's overlap was minimal (9%). These results, consistent with findings for ApoE3 (Tables S5 and S6), align with the inter-domain binding model proposed in [16]. Specifically, the involvement of N-terminal residues in full-length simulations confirms that EZ-482—and similarly the tested nutraceuticals—occupies an inter-domain groove rather than a pocket strictly confined to the C-terminal region.

Table 3. Residue-level agreement with Jaccard index and Sørensen–Dice coefficient between SwissDock and Schrödinger Maestro for truncated C-term (216–299) and ApoE4 (1–299) and ligands. Percentage of shared interacting residues.

Region	Ligand	Jaccard Index	Sørensen–Dice Coefficient	Residues Concordant	Characteristic
C-terminal (216–299)	EZ-482	0	0	0%	No residue overlap
	Polydatin	0.12	0.21	12%	Minimal interaction
	Trans-resveratrol	0.05	0.095	5%	Minimal interaction
	Luteolin	0.058	0.11	5.8%	Minimal interaction
	PEA	0.38	0.55	38%	Highest potential
ApoE4 (1–299)	EZ-482	0.36	0.52	36%	Reference ligand
	Polydatin	0.34	0.48	34%	Highest potential
	Trans-resveratrol	0.27	0.30	27%	Strong interaction
	Luteolin	0.23	0.30	23%	Moderate interaction
	PEA	0.09	0.17	9%	Minimal interaction

Residue-level comparison within the HDX-MS-defined EZ-482 cavity (229–265) revealed a stark divergence between the interaction patterns predicted by SwissDock and Schrödinger Maestro Glide (Table 4). While SwissDock consistently identified Leu229 as the sole interaction point for all ligands, Schrödinger detected residue clusters in the central portion of the segment, primarily involving Lys242, Glu245, Gln249, Leu252, and Gln253 (Figure 2A,B). The total lack of residue-level overlap between the two platforms suggests that the 229–265 region does not constitute an autonomous structural binding

pocket when isolated from the surrounding protein framework. Instead, this segment likely represents a broader interaction microenvironment whose functional architecture emerges only within the spatial context of the C-terminal domain. This interpretation aligns with the role of the C-terminal region in providing the hydrophobic scaffolding necessary for lipoprotein association and structural stabilization [38]. Consequently, the isolation of this short peptide disrupts the native structural elements required to form a functional binding site.

Table 4. Amino acid residue comparison of nutraceutical interactions for HDX-MS EZ-482 binding cavity (229–265) across docking platforms. Shared residues are highlighted in bold.

Region	Ligands	a.a. Detected by SwissDock	a.a. Detected by Schrödinger Maestro Glide
HDX-MS EZ-482 (229–265)	EZ-482	Leu229	Lys242 Leu243 Glu245 Gln246 Gln249 Leu252 Gln253 Ala256 Ala257
	Polydatin	Leu229	Arg240 Ala241 Lys242 Glu244 Glu245 Gln248 Gln249 Leu252 Gln253
	Trans-Resveratrol	Leu229 Asp230 Glu231	Lys242 Glu245 Gln246 Gln249 Leu252 Gln253 Ala256
	Luteolin	Leu229	Lys242 Glu245 Gln246 Gln249 Leu252 Gln253
	PEA	Leu229	Lys242 Glu245 Gln246 Gln249 Leu252 Gln253 Ala256

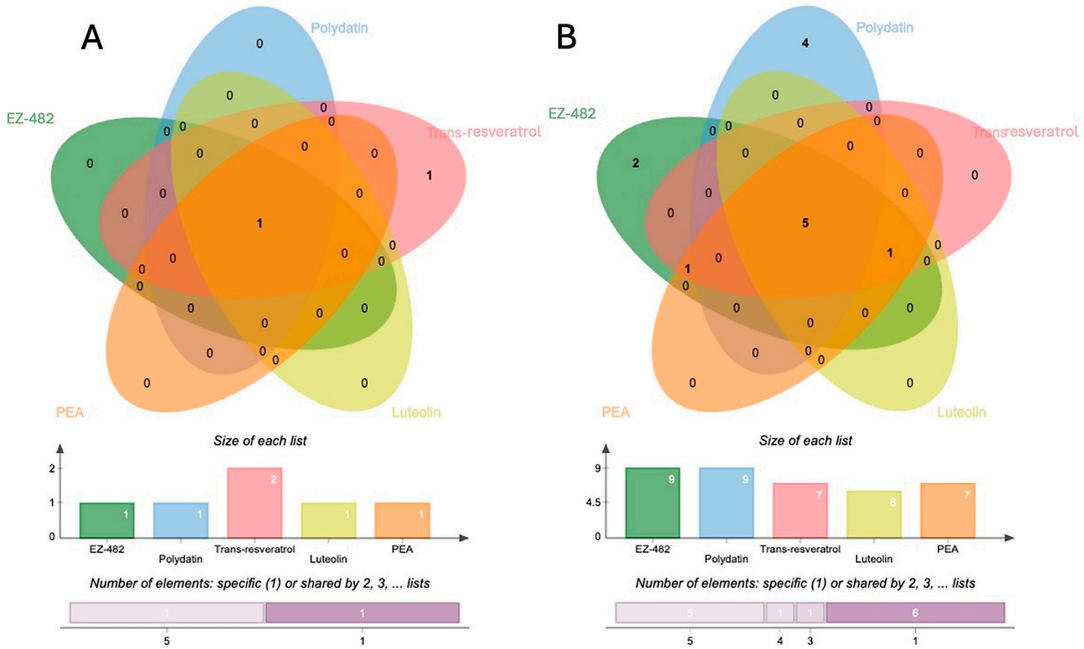

Figure 2. Venn diagram illustrating amino acid residues recurrently identified across all analyzed ligands within the HDX-MS EZ-482 binding cavity (229–265), binding cavity by SwissDock (**A**) and Schrödinger Maestro Glide (**B**).

Representative docking poses for the HDX-MS EZ-482 cavity (229–265), obtained from both SwissDock and Schrödinger Maestro Glide, are displayed in Figure 3 (panels a–e and f–j, respectively). Table 5 reports the specific residues forming the C-terminal (216–299) interaction region for each ligand.

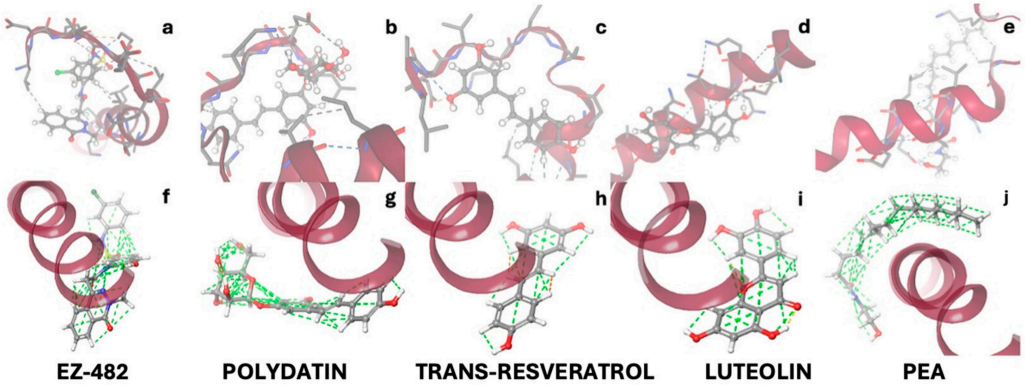

Figure 3. Docking on HDX-MS EZ-482 binding cavity (229–265). Docking poses with SwissDock for (**a**) EZ-482, (**b**) polydatin, (**c**) trans-resveratrol, (**d**) luteolin, and (**e**) PEA. Dashed lines indicate predicted non-covalent interactions, including hydrogen bonds and electrostatic contacts. Docking poses with Schrödinger Maestro Glide for (**f**) EZ-482, (**g**) polydatin, (**h**) trans-resveratrol, (**i**) luteolin, and (**j**) PEA. Green dashed lines indicate predicted non-covalent interactions, including hydrogen bonds and π–cation contacts. The protein backbone is shown in cartoon representation, and ligands are displayed in stick format.

Table 5. Amino acid residue comparison of nutraceutical interactions for C-terminal (216–299) across docking platforms. Shared residues are highlighted in bold.

Region	Ligands	a.a. Detected by SwissDock	a.a. Detected by Schrödinger Maestro Glide
C-terminal (216–299)	EZ-482	Met221 Thr225 Leu229	Glu231 Lys233 Val239 Lys242 Leu243 Glu245 Gln246 Gln249 Gln279 Val280 Glu281 Lys282 Val283 Glu287 Gly288 Ala291 Ala292 Pro293 Val294
	Polydatin	Met221 Thr225 Asp227 Arg228 **Leu229 Val280 Glu281**	**Leu229** Glu231 Val232 Lys233 Val239 Lys242 Leu243 Glu245 Gln246 Gln249 Gln253 **Val280 Glu281** Lys282 Val283 Glu287 Gly288 Ala291 Ala292 Pro293 Val294
	Trans-Resveratrol	Asp227 Arg228 **Leu229** Thr289	**Leu229** Glu231 Val239 Lys242 Leu243 Glu245 Gln246 Gln249 Gln253 Glu281 Val283 Glu287 Gly288 Ala291 Ala292 Pro293 Val294
	Luteolin	Thr225 Asp227 Arg228 **Leu229**	**Leu229** Lys242 Leu243 Glu245 Gln246 Gln249 Glu287 Gly288 Thr289 Ser290 Ala291 Ala292 Pro293 Val294
	PEA	Arg228 **Leu229** Asp230 **Glu231** Gly278 Gln279 **Val280 Glu281** Lys282 **Val283 Gln284** Ala285 **Ala286 Glu287 Gly288** Thr289 Ser290 **Ala291 Ala292 Pro293**	**Leu229 Glu231** Val232 Lys233 Val239 Lys242 Leu243 Glu245 Gln246 Gln249 Gln253 **Val280 Glu281 Val283 Gln284 Ala286 Glu287 Gly288 Ala291 Ala292 Pro293** Val294 Asp297

For the reference ligand EZ-482, no overlapping residues were identified between the two platforms. In contrast, Polydatin showed consistency for three residues: Leu229, Val280, and Glu281, while trans-resveratrol and luteolin shared only a single common residue, Leu229. Notably, PEA exhibited the highest level of concordance, with twelve residues consistently identified by both platforms: Leu229, Glu231, Val280, Glu281, Val283, Gln284,

Ala286, Glu287, Gly288, Ala291, Ala292, and Pro293. This strong agreement underscores the preferential affinity of PEA for the C-terminal hydrophobic domain.

Notably, this region is shared with all the ApoEs. Within this region, Leu229 was the only residue recurrently identified across EZ-482 and all nutraceutical ligands in the SwissDock analysis. (Figure 4A). Schrödinger Maestro Glide identified eleven amino acids commonly shared between EZ-482 and nutraceuticals: Lys242, Leu243, Glu245, Gln246, Gln249, Glu287, Gly288, Ala291, Ala292, Pro293 and Val294 (Figure 4B).

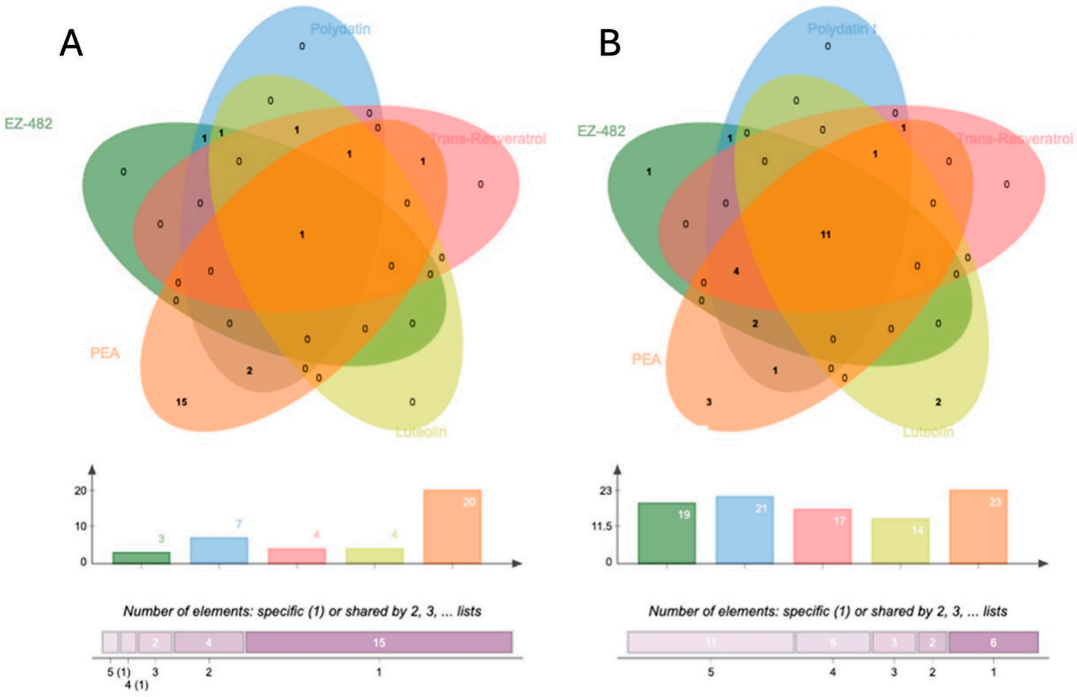

Figure 4. Venn diagram illustrating amino acid residues recurrently identified across all analyzed ligands within the C-terminal ApoE (216–299) binding cavity by SwissDock (**A**) and Schrödinger Maestro Glide (**B**).

Representative docking poses for ApoE C-terminal (216–299) obtained from both SwissDock and Schrödinger Maestro Glide are displayed in Figure 5 (Panels a–e and f–j, respectively).

Table 6 reports the amino acid residues constituting the ApoE4 (1–299) as identified by SwissDock and Schrödinger Maestro Glide for each ligand. In particular, for EZ-482 fourteen were shared in the two platforms, the Lys1, Val2, Ala5, Val6, Trp34, Leu37, Arg38, Trp39, Gln41, Arg145, Lys146, Leu149, Met221, and Thr225; thirteen for the polydatin, the Lys1, Val2, Ala5, Val6, Thr8, Glu9, Arg38, Gln41, Arg145, Lys146, Leu149, Met221, Thr225; eight for trans-resveratrol and luteolin, the Lys1, Ala5, Val6, Thr8, Glu9, Arg38, Gln41, Arg145, and Lys1, Val2, Ala5, Arg38, Gln41, Arg134, Arg145, and Thr225 respectively, while only three were identified for PEA, the Ala5, Thr8, and Arg228. A common amino acid signature shared among platforms and nutraceuticals emerges: Lys1, Ala5, Arg145. The same a.a. were identified recently to be crucial for genkwanin and kaempferol [41,42]. Notably, in animal model studies, exogenously expressing human ApoE4 revealed its aggregation and deposition with Aβ. It has been shown that blocking this binding with a mimetic peptide corresponding to the 12–28 fragment of Aβ counteracts key in vivo and in vitro pathological effects of Aβ [11].

Table 6. Amino acid residue comparison of nutraceutical interactions for ApoE4 (1–299) across docking platforms. Shared residues are highlighted in bold.

Region	Ligands	a.a. Detected by SwissDock	a.a. Detected by Schrödinger Maestro Glide
ApoE4 (1–299)	EZ-482	**Lys1 Val2** Glu3 Gln4 **Ala5 Val6** Phe33 **Trp34 Leu37** **Arg38 Trp39** Val40 **Gln41** Thr42 Val111 Arg114 Arg134 Leu137 Ala138 Ser139 His140 Leu141 Arg142 Lys143 Leu144 **Arg145 Lys146** Leu148 **Leu149 Met221** **Thr228** Leu229	**Lys1 Val2 Ala5** **Val6** Thr8 Glu9 Arg15 **Trp34 Leu37** **Arg38 Trp39 Gln41** **Arg145 Lys146 Leu149** **Met221** Gly222 Ser223 Arg224 **Thr225** Arg228
	Polydatin	**Lys1 Val2** Glu3 Gln4 **Ala5 Val6** Glu7 **Thr8 Glu9** Pro10 **Arg38** Val40 **Gln41** Thr42 Arg134 Val135 Arg136 Leu137 Ala138 Ser139 Leu141 Arg142 **Arg145** **Lys146 Leu149 Met221 Thr225** Asp227 Arg228 Leu229 Val280 Glu281	**Lys1 Val2 Ala5** **Val6 Thr8 Glu9** Trp34 Leu37 **Arg38** Trp39 **Gln41 Arg145 Lys146 Leu149** **Met221** Gly222 Ser223 Arg224 **Thr225**
	Trans-Resveratrol	**Lys1** Val2 Glu3 Gln4 **Ala5 Val6** Glu7 **Thr8 Glu9 Arg38 Gln41** Val135 Leu137 Ala138 Ser139 His140 Leu141 Arg142 Lys143 **Arg145** Arg228 Leu229 Thr289	**Lys1 Ala5 Val6** **Thr8 Glu9** Trp34 Leu37 **Arg38 Gln41** Arg134 **Arg145** Leu149 Met221 Gly222 Thr225
	Luteolin	**Lys1 Val2** Glu3 Gln4 **Ala5** Leu37 **Arg38 Gln41** Thr42 Leu43 Leu133 **Arg134** Val135 Arg136 Leu137 Ala138 Ser139 Leu141 Arg142 Lys143 **Arg145** Lys146 **Thr225** Asp227 Arg228 Leu229	**Lys1 Val2 Ala5** Val6 Thr8 Glu9 **Arg38 Gln41 Arg134 Arg145** Leu149 Met221 Gly222 Ser223 Arg224 **Thr225**
	PEA	Glu3 Gln4 **Ala5** Glu7 **Thr8** Glu11 Leu14 Val135 Arg136 Ser139 Arg142 Lys143 **Lys146** Arg150 **Arg228** Leu229 Asp230 Glu231 Gln279 Val280 Glu281 Lys282 Val283 Gln284 Ala286 Glu287 Gly288 Thr289 Ser290 Ala291 Ala292 Pro293 Val294	Lys1 Val2 **Ala5** Val6 **Thr8** Glu9 Phe33 Trp34 Asp35 Leu37 Arg38 Gln41 Arg145 **Lys146** Leu148 Leu149 Met221 Gly222 Ser223 Arg224 Thr225 **Arg228**

Furthermore, within the full-length ApoE4 (1–299) structure, shared by the EZ-482 and the nutraceuticals SwissDock identified six a.a. recognized as Glu3, Gln4, Ala5, Ser139, Arg142 and Leu229 (Figure 6A); whereas Schrödinger Maestro Glide highlighted twelve a.a. common shared among EZ-482 and nutraceuticals: Lys1, Ala5, Val6, Thr8, Glu9, Arg38, Gln41, Arg145, Leu149, Met221, Gly222 and Thr225 (Figure 6B).

Representative docking poses for ApoE4 (1–299) obtained from SwissDock and Schrödinger Maestro Glide are displayed in Figure 7 (Panels a–e and f–j, respectively). For ApoE3, see Figure S2.

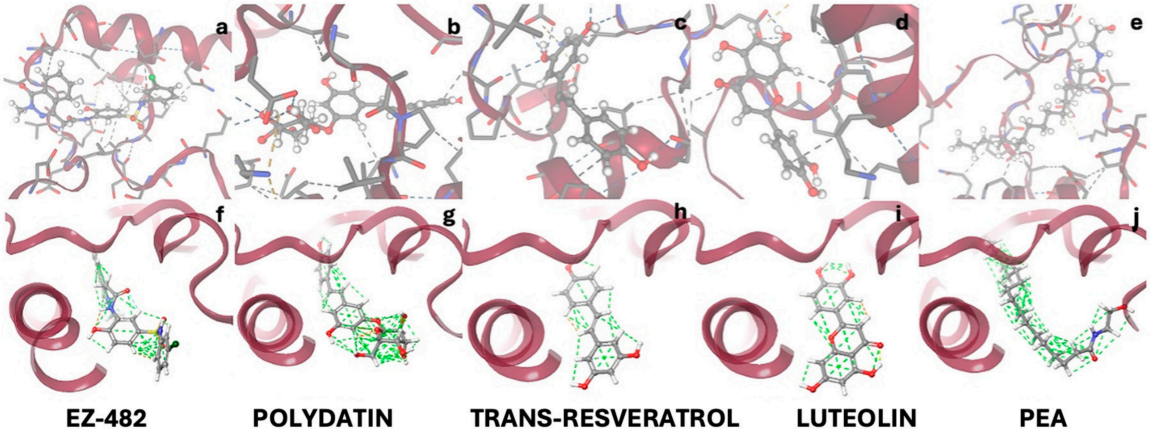

Figure 5. Docking on the C-terminal (216–299). Docking poses with SwissDock for (**a**) EZ-482, (**b**) polydatin, (**c**) trans-resveratrol, (**d**) luteolin and (**e**) PEA. Dashed lines indicate predicted non-covalent interactions, including hydrogen bonds and electrostatic contacts. Docking poses with Schrödinger Maestro Glide for (**f**) EZ-482, (**g**) polydatin, (**h**) trans-resveratrol, (**i**) luteolin and (**j**) PEA. Green dashed lines indicate predicted non-covalent interactions, including hydrogen bonds and π–cation contacts. The protein backbone is shown in cartoon representation, and ligands are displayed in stick format.

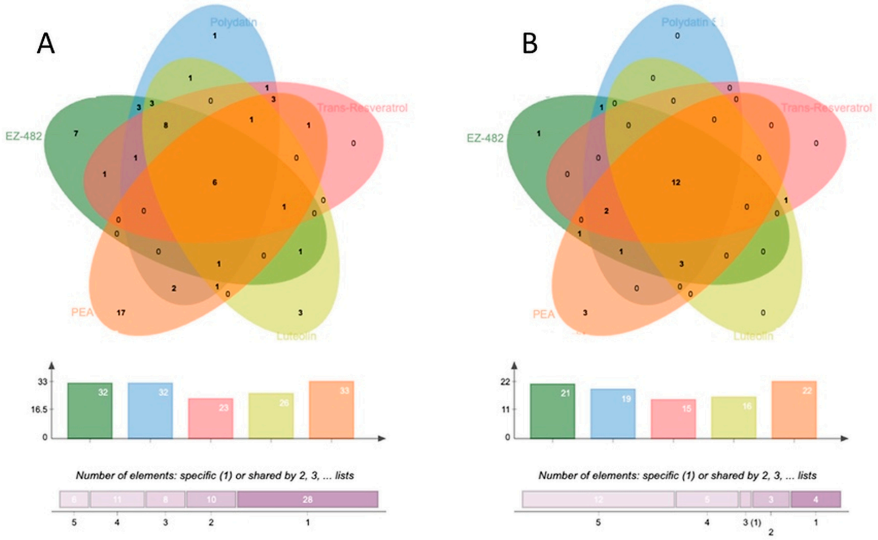

Figure 6. Venn diagram illustrating amino acid residues recurrently identified across all analyzed ligands within the full-length ApoE4 (1–299) by SwissDock (**A**) and Schrödinger Maestro Glide (**B**).

Comparative analysis of residue recurrence across structural constructs demonstrates a context-dependent modulation of docking behavior. In the full-length ApoE4 structure, residue-level overlap between SwissDock and Schrödinger Maestro remains partial yet consistent, suggesting that the whole protein architecture contributes to stabilizing ligand accommodation. Docking simulations rely on static protein conformations and simplified treatment of solvent and entropic contributions [43]. Recent experimental evidence supports this inter-domain binding model. The ApoE4-specific C112R substitution has been shown to induce long-range conformational rearrangements (>15 Å), resulting in a distinct V-shaped dimeric structure with increased aggregation propensity [44]. These findings indicate that ApoE4 structural behavior is governed by global conformational reorganization rather than localized sequence effects. In addition, quantitative HDX-MS studies have demonstrated that ApoE4 exhibits enhanced conformational heterogeneity and faster deuterium exchange kinetics compared to ApoE3, reflecting increased structural flexibility and reduced stability [45]. Notably, this conformational heterogeneity is more

pronounced in the full-length protein than in isolated domains, highlighting the importance of inter-domain coupling in shaping ApoE4 structural dynamics.

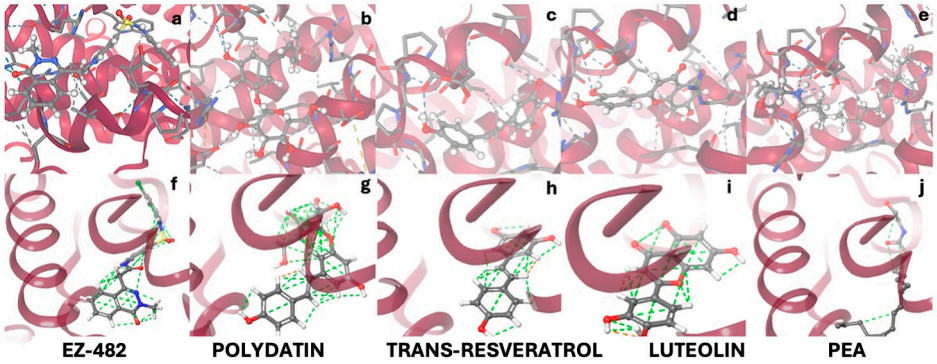

Figure 7. Docking on ApoE4 (1–299). Docking poses with SwissDock for (**a**) EZ-482, (**b**) polydatin, (**c**) trans-resveratrol, (**d**) luteolin and (**e**) PEA. Dashed lines indicate predicted non-covalent interactions, including hydrogen bonds and electrostatic contacts. Docking poses with Schrödinger Maestro Glide for (**f**) EZ-482, (**g**) polydatin, (**h**) trans-resveratrol, (**i**) luteolin and (**j**) PEA. Green dashed lines indicate predicted non-covalent interactions, including hydrogen bonds and π–cation contacts. The protein backbone is shown in cartoon representation, and ligands are displayed in stick format.

3.5. Translational Implications for Structure-Based Drug Design

The residue-level concordance analysis across both docking platforms suggests three potential implications for structure-based design of ApoE4-targeted compounds. First, the recurrent amino acid signature shared between EZ-482 and the nutraceuticals in the full-length ApoE4 (1–299) construct (Lys1, Ala5, Arg145) delineates a consistently observed interaction region that may serve as a basis for pharmacophore model construction, in line with previous work on ApoE4 structure correctors where pharmacophore models were derived from docking-based interaction patterns to guide analog optimization [46,47]. Second, the flavone scaffold of luteolin and the stilbene scaffold of polydatin represent chemically tractable starting points for scaffold-hopping campaigns aimed at improving potency, metabolic stability, and blood–brain barrier permeability. This view is supported by the recent identification of isobavachin, a bioavailable flavonoid, as an ApoE4 structure corrector through docking-based workflows with biophysical validation [48]. Furthermore, additional flavonoids such as naringenin and diosmetin modulate apoE-related pathways and ApoE4-induced APP processing, underscoring the relevance of this scaffold class for ApoE4-targeted design [49,50]. Third, the observation that only full-length ApoE4 (1–299) yields consistent cross-platform docking rankings, whereas truncated constructs do not, indicates that inclusion of the inter-domain structural context is important for accurately modeling ligand accommodation at the C-terminal site. This is consistent with fragment-based and biophysical studies showing that ApoE4 stabilization and allosteric modulation depend on the global domain architecture of the protein.

3.6. Dynamic Light Scattering Analysis of the ApoE4-Containing Lipoprotein System

Dynamic light scattering (DLS) was employed to characterize the macromolecular assemblies and their interactions, as shifts in ζ-potential and hydrodynamic diameter directly reflect intermolecular effects in solution [51]. The protein–lipid interaction was first assessed by a change in the ζ-potential of oxLDL, which shifted from −2.93 mV to approximately −11 mV upon complexation with ApoE4. To isolate the electrostatic contribution of the tested nutraceuticals, perturbations were expressed relative to the ApoE4–oxLDL baseline (−10.97 mV). The addition of the ligands induced ligand-dependent shifts toward less negative values, indicating a partial neutralization or shielding of surface

charges at the lipoprotein interface [52]. Notably, the luteolin-induced shift (+2.15 mV) was accompanied by a significant reduction in the hydrodynamic diameter of the assemblies. This suggests that luteolin triggers a structural compaction of the lipoprotein complex, potentially stabilizing the ApoE4 conformation and mitigating its pathological expansion on the oxLDL surface. Detailed results are summarized in Table 7.

Table 7. Ligand-induced shifts in ζ-potential of the ApoE4-containing lipoprotein system measured by dynamic light scattering (DLS). Values are expressed relative to the ApoE4 + oxLDL baseline (−10.97 mV).

Compound	Mean ζ-Potential (mV)	Standard Deviation ζ-Potential (mV)	Δζ-Potential (mV)
Polydatin	−10.5	±0.5	−0.46
Trans-resveratrol	−11.70	±0.3	−0.73
Luteolin	−8.82	±1.02	**+2.15**
PEA	−9.92	±0.73	**+1.05**

The addition of the nutraceuticals results in less negative ζ-potential values, indicating partial neutralization or shielding of surface charges at the lipoprotein interface, suggesting ligand-dependent perturbations of the electrostatic environment surrounding the particles [52]. Although ζ-potential measurements do not directly measure ligand binding, these results are consistent with the hypothesis that the tested compounds modulate the physicochemical properties of the ApoE4-containing lipoprotein system. These observations are consistent with a structure-dependent mechanism in which ligand binding modulates the global conformational state of ApoE4. Given that conformational rearrangements in ApoE4 directly influence surface exposure and charge distribution, the ligand-induced perturbations observed in ζ-potential measurements likely reflect underlying structural changes in the protein–lipoprotein complex [44,45]. Interestingly, compounds predicted by docking to interact with the ApoE4 C-terminal region, particularly luteolin, also produced detectable electrostatic perturbations in the DLS measurements. These observations therefore provide an independent physicochemical readout consistent with ligand-dependent modulation of the ApoE4-associated system predicted by the computational analysis. It is worth mentioning that formulations containing PEA and luteolin are commercially available, and it is proposed that they counteract cognitive decline in the early stages of AD [52–56].

3.7. Limitations and Future Perspectives

The present study utilizes a dual-platform docking strategy and dynamic light scattering to explore the interaction between nutraceuticals and ApoE4. While these results provide a promising framework for identifying ApoE4-targeting candidates, we acknowledge the inherent limitations of these methods. Docking represents a static computational snapshot and does not capture the conformational flexibility of the protein–ligand system. Similarly, ζ-potential measurements serve as an indirect indicator of surface charge perturbation. Consequently, our findings should be interpreted as predictive of putative interactions that prioritize compounds for future biophysical validation. Future experimental efforts, including Surface Plasmon Resonance (SPR) and Isothermal Titration Calorimetry (ITC), will be essential to rigorously assess the binding kinetics, thermodynamic stability, and long-term interaction dynamics of these candidates.

4. Conclusions

The experimental ranking of ζ-potential perturbations is broadly consistent with the interaction trends predicted by full-length ApoE4 docking. Collectively, these findings suggest ligand-dependent modulation of the ApoE4–lipoprotein electrostatic environment

and underscore the mandatory role of full structural context in ApoE4 analysis. Our data suggest that localized conformational shifts may contribute to pathological behavior, identifying luteolin and PEA as promising scaffolds for structure-based drug design and targeted nutraceutical interventions in Alzheimer's disease. These results support a structure-dependent mechanism linking ApoE4 conformational dynamics, surface charge modulation, and aggregation-prone behavior.

Supplementary Materials: The following supporting information can be downloaded at: https://www.mdpi.com/article/10.3390/biomedinformatics6030029/s1. Figure S1: Structural validation of human ApoE3 was performed using the ProSA web server; Figure S2: Docking on ApoE3 (1-299); Table S1: Comparative overview of SwissDock (Attracting Cavities) and Schrödinger Maestro Glide docking platforms; Table S2: Reported plasma concentrations of the nutraceutical compounds used in this study after oral administration compared with the stabilized concentrations employed in the experimental samples; Table S3: Cross platform correlation analysis of normalized docking scores ($\Delta\Delta G = \Delta G\_lig - \Delta G\_EZ\text{-}482$) for ApoE3 isoform; Table S4: Docking-derived interaction energies for nutraceutical compounds within the EZ-482 binding cavity of ApoE3 (1-299) isoforms as predicted by SwissDock and Schrödinger Maestro Glide; Table S5: Residue-level comparison of ligand interactions predicted for ApoE3 isoform by SwissDock and Schrödinger Maestro Glide; Table S6: Residue level comparison of binding pocket interactions for ApoE3 (1-299) across docking platforms.

Author Contributions: Conceptualization, E.C. and G.F.S.; methodology, G.F.S. and C.F.; software, G.F.S.; validation, D.S.; formal analysis, G.F.S. and D.S.; investigation, G.F.S. and D.S.; resources, E.C.; data curation, G.F.S. and C.F.; writing—original draft preparation, E.C.; writing—review and editing, E.C.; visualization, E.C.; supervision, E.C.; funding acquisition, E.C. All authors have read and agreed to the published version of the manuscript.

Funding: PNRR Project supported this research: H23C22000370006-T4Y S5G4PP1 to E.C.

Institutional Review Board Statement: Not applicable.

Informed Consent Statement: Not applicable.

Data Availability Statement: The original contributions presented in this study are included in the article/Supplementary Material. Further inquiries can be directed to the corresponding author.

Conflicts of Interest: The authors declare no conflicts of interest.

Abbreviations

The following abbreviations are used in this manuscript:

a.a.	Amino acids
AD	Alzheimer Disease
ApoE	Apolipoprotein E
Aβ	Amyloid Beta
BSA	Bovine Serum Albumin
DLS	Dynamic Light Scattering
DMSO	Di Methyl Sulf-Oxide
DPBS	Dulbecco Phosphate-Buffered Saline
HDX-MS	Hydrogen/Deuterium eXchange Mass Spectrometry
NMR	Nuclear magnetic resonance
oxLDL	Oxidized Low-Density Lipoproteins
PEA	Palmitoylethanolamide
ProSA	Protein Structure Analysis web server
r	Pearson
SP	Standard Precision
ΔG	Binding free energy

ΔΔG	Normalized binding energy difference
ϱ	Spearman

References

1. Abrego-Guandique, D.M.; Saraceno, G.F.; Cannataro, R.; Manzzo de Burnside, M.; Caroleo, M.C.; Cione, E. Apolipoprotein E and Alzheimer's Disease in Italian Population: Systematic Review and Meta-Analysis. *Brain Sci.* **2024**, *14*, 908. [CrossRef]
2. Al-Ghraiybah, N.F.; Alkhalifa, A.E.; Itokazu, Y.; Farr, T.O.; Perez, N.C.; Ali, H.; Kaddoumi, A. Apolipoprotein E4 in Alzheimer's Disease: Role in Pathology Lipid Metabolism and Drug Treatment. *Int. J. Mol. Sci.* **2026**, *27*, 1004. [CrossRef]
3. Holtzman, D.M.; Herz, J.; Bu, G. Apolipoprotein E and apolipoprotein E receptors: Normal biology and roles in Alzheimer disease. *Cold Spring Harb. Perspect. Med.* **2012**, *2*, a006312. [CrossRef]
4. Bien-Ly, N.; Gillespie, A.K.; Walker, D.; Yoon, S.Y.; Huang, Y. Reducing human apolipoprotein E levels attenuates age-dependent Aβ accumulation in mutant human amyloid precursor protein transgenic mice. *J. Neurosci. Off. J. Soc. Neurosci.* **2012**, *32*, 4803–4811. [CrossRef] [PubMed]
5. Jones, P.B.; Adams, K.W.; Rozkalne, A.; Spires-Jones, T.L.; Hshieh, T.T.; Hashimoto, T.; von Armin, C.A.; Mielke, M.; Bacskai, B.J.; Hyman, B.T. Apolipoprotein E: Isoform specific differences in tertiary structure and interaction with amyloid-β in human Alzheimer brain. *PLoS ONE* **2011**, *6*, e14586. [CrossRef] [PubMed]
6. Kanekiyo, T.; Xu, H.; Bu, G. ApoE and Aβ in Alzheimer's disease: Accidental encounters or partners? *Neuron* **2014**, *81*, 740–754. [CrossRef]
7. Raulin, A.C.; Doss, S.V.; Trottier, Z.A.; Ikezu, T.C.; Bu, G.; Liu, C.C. ApoE in Alzheimer's disease: Pathophysiology and therapeutic strategies. *Mol. Neurodegener.* **2022**, *17*, 72. [CrossRef]
8. Weisgraber, K.H.; Rall, S.C., Jr.; Mahley, R.W. Human E apoprotein heterogeneity. Cysteine-arginine interchanges in the amino acid sequence of the apo-E isoforms. *J. Biol. Chem.* **1981**, *256*, 9077–9083. [CrossRef]
9. Roses, A.D. Apolipoprotein E alleles as risk factors in Alzheimer's disease. *Annu. Rev. Med.* **1996**, *47*, 387–400. [CrossRef] [PubMed]
10. Bellenguez, C.; Küçükali, F.; Jansen, I.E.; Kleineidam, L.; Moreno-Grau, S.; Amin, N.; Naj, A.C.; Campos-Martin, R.; Grenier-Boley, B.; Andrade, V.; et al. New insights into the genetic etiology of Alzheimer's disease and related dementias. *Nat. Genet.* **2022**, *54*, 412–436. [CrossRef]
11. Liu, C.C.; Zhao, N.; Fu, Y.; Wang, N.; Linares, C.; Tsai, C.W.; Bu, G. ApoE4 Accelerates Early Seeding of Amyloid Pathology. *Neuron* **2017**, *96*, 1024–1032.e3. [CrossRef] [PubMed]
12. Xia, Z.; Prescott, E.E.; Urbanek, A.; Wareing, H.E.; King, M.C.; Olerinyova, A.; Dakin, H.; Leah, T.; Barnes, K.A.; Matuszyk, M.M.; et al. Co-aggregation with Apolipoprotein E modulates the function of Amyloid-β in Alzheimer's disease. *Nat. Commun.* **2024**, *15*, 4695. [CrossRef] [PubMed]
13. Saraceno, G.F.; Cione, E. Multiple Bio-Computational Tools Emerge as Valid Approach in the Assessment of Apolipoproteins Pathogenicity Related Mutations. *BioMedInformatics* **2025**, *5*, 16. [CrossRef]
14. Saraceno, G.F.; Abrego-Guandique, D.M.; Cannataro, R.; Caroleo, M.C.; Cione, E. Machine Learning Approach to Identify Case-Control Studies on ApoE Gene Mutations Linked to Alzheimer's Disease in Italy. *BioMedInformatics* **2024**, *4*, 600–622. [CrossRef]
15. Chen, H.K.; Liu, Z.; Meyer-Franke, A.; Brodbeck, J.; Miranda, R.D.; McGuire, J.G.; Pleiss, M.A.; Ji, Z.S.; Balestra, M.E.; Walker, D.W.; et al. Small molecule structure correctors abolish detrimental effects of apolipoprotein E4 in cultured neurons. *J. Biol. Chem.* **2012**, *287*, 5253–5266. [CrossRef]
16. Mondal, T.; Wang, H.; DeKoster, G.T.; Baban, B.; Gross, M.L.; Frieden, C. ApoE: In Vitro Studies of a Small Molecule Effector. *Biochemistry* **2016**, *55*, 2613–2621. [CrossRef]
17. Mamotte, C.D.; Sturm, M.; Foo, J.I.; van Bockxmeer, F.M.; Taylor, R.R. Comparison of the LDL-receptor binding of VLDL and LDL from apoE4 and apoE3 homozygotes. *Am. J. Physiol.* **1999**, *276*, E553–E557. [CrossRef]
18. Akyol, O.; Chiang, H.H.; Burns, A.R.; Yang, C.Y.; Woodside, D.G.; Sawamura, T.; Sánchez-Quesada, J.L.; Gotto, A.M.; Chen, C.H. LDL atherogenicity determined by size, density, oxidation, apolipoprotein(a), and electronegativity: An updated review. *Front. Cardiovasc. Med.* **2025**, *12*, 1649759. [CrossRef]
19. Safieh, M.; Korczyn, A.D.; Michaelson, D.M. ApoE4: An emerging therapeutic target for Alzheimer's disease. *BMC Med.* **2019**, *17*, 64. [CrossRef]
20. Belaidi, A.A.; Bush, A.I.; Ayton, S. Apolipoprotein E in Alzheimer's disease: Molecular insights and therapeutic opportunities. *Mol. Neurodegener.* **2025**, *20*, 47. [CrossRef]
21. Abrego-Guandique, D.M.; Bonet, M.L.; Caroleo, M.C.; Cannataro, R.; Tucci, P.; Ribot, J.; Cione, E. The Effect of Beta-Carotene on Cognitive Function: A Systematic Review. *Brain Sci.* **2023**, *13*, 1468. [CrossRef]
22. Yuan, S.F.; Long, C.H.; Zhang, X.; Yuan, M.; Li, J.; Wu, H.G. Causal Effects of Circulating Micronutrients on Cognitive Function: Evidence from a Mendelian Randomization Study. *Brain Behav.* **2025**, *15*, e70488. [CrossRef]

23. Kou, J.J.; Shi, J.Z.; He, Y.Y.; Hao, J.J.; Zhang, H.Y.; Luo, D.M.; Song, J.K.; Yan, Y.; Xie, X.M.; Du, G.H.; et al. Luteolin alleviates cognitive impairment in Alzheimer's disease mouse model via inhibiting endoplasmic reticulum stress-dependent neuroinflammation. *Acta Pharmacol. Sin.* **2022**, *43*, 840–849. [CrossRef] [PubMed]
24. Ding, Z.; Hou, Q.; Shao, N.; Gao, W.; Cai, B.; Hu, S. Polydatin Attenuates Cognitive Deficits and Neuroinflammation by Inhibiting the P2X7/NLRP1 Inflammasome Pathway in APP/PS1 Mice and Aβ-Treated HT22 Cells. *Mol. Neurobiol.* **2025**, *63*, 311. [CrossRef] [PubMed]
25. Cicero, A.F.G.; Ruscica, M.; Banach, M. Resveratrol and cognitive decline: A clinician perspective. *Arch. Med. Sci. AMS* **2019**, *15*, 936–943. [CrossRef]
26. Colizzi, M.; Bortoletto, R.; Colli, C.; Bonomo, E.; Pagliaro, D.; Maso, E.; Di Gennaro, G.; Balestrieri, M. Therapeutic effect of palmitoylethanolamide in cognitive decline: A systematic review and preliminary meta-analysis of preclinical and clinical evidence. *Front. Psychiatry* **2022**, *13*, 1038122. [CrossRef]
27. Wiederstein, M.; Sippl, M.J. ProSA-web: Interactive web service for the recognition of errors in three-dimensional structures of proteins. *Nucleic Acids Res.* **2007**, *35*, W407–W410. [CrossRef]
28. Grosdidier, A.; Zoete, V.; Michielin, O. SwissDock a protein-small molecule docking web service based on EADock DSS. *Nucleic Acids Res.* **2011**, *39*, W270–W277. [CrossRef]
29. Grosdidier, A.; Zoete, V.; Michielin, O. EADock: Docking of small molecules into protein active sites with a multiobjective evolutionary optimization. *Proteins* **2007**, *67*, 1010–1025. [CrossRef]
30. Friesner, R.A.; Banks, J.L.; Murphy, R.B.; Halgren, T.A.; Klicic, J.J.; Mainz, D.T.; Repasky, M.P.; Knoll, E.H.; Shelley, M.; Perry, J.K.; et al. Glide: A new approach for rapid accurate docking and scoring. 1. Method and assessment of docking accuracy. *J. Med. Chem.* **2004**, *47*, 1739–1749. [CrossRef] [PubMed]
31. Friesner, R.A.; Murphy, R.B.; Repasky, M.P.; Frye, L.L.; Greenwood, J.R.; Halgren, T.A.; Sanschagrin, P.C.; Mainz, D.T. Extra precision glide: Docking and scoring incorporating a model of hydrophobic enclosure for protein-ligand complexes. *J. Med. Chem.* **2006**, *49*, 6177–6196. [CrossRef]
32. van Zundert, G.C.P.; Moriarty, N.W.; Sobolev, O.V.; Adams, P.D.; Borrelli, K.W. Macromolecular refinement of X-ray and cryoelectron microscopy structures with Phenix/OPLS3e for improved structure and ligand quality. *Structure* **2021**, *29*, 913–921.e4. [CrossRef]
33. Sastry, G.M.; Adzhigirey, M.; Day, T.; Annabhimoju, R.; Sherman, W. Protein and ligand preparation: Parameters protocols and influence on virtual screening enrichments. *J. Comput. Aided Mol. Des.* **2013**, *27*, 221–234. [CrossRef] [PubMed]
34. Blanes-Mira, C.; Fernández-Aguado, P.; de Andrés-López, J.; Fernández-Carvajal, A.; Ferrer-Montiel, A.; Fernández-Ballester, G. Comprehensive Survey of Consensus Docking for High-Throughput Virtual Screening. *Molecules* **2022**, *28*, 175. [CrossRef] [PubMed]
35. Palacio-Rodríguez, K.; Lans, I.; Cavasotto, C.N.; Cossio, P. Exponential consensus ranking improves the outcome in docking and receptor ensemble docking. *Sci. Rep.* **2019**, *9*, 5142. [CrossRef]
36. Tutone, M.; Almerico, A.M. Computational Strategies Reshaping Modern Drug Discovery. *Molecules* **2026**, *31*, 200. [CrossRef]
37. Röhrig, U.F.; Goullieux, M.; Bugnon, M.; Zoete, V. Attracting Cavities 2.0: Improving the Flexibility and Robustness for Small-Molecule Docking. *J. Chem. Inf. Model.* **2023**, *63*, 3925–3940. [CrossRef]
38. Wang, S.; Xu, X.; Pan, C.; Guo, Q.; Li, Q.; Wan, S.; Li, Z.; Zhang, J.; Wu, X. Identification of New EGFR Inhibitors by Structure-Based Virtual Screening and Biological Evaluation. *Int. J. Mol. Sci.* **2024**, *25*, 1887. [CrossRef] [PubMed]
39. Scardino, V.; Bollini, M.; Cavasotto, C.N. Combination of pose and rank consensus in docking-based virtual screening: The best of both worlds. *RSC Adv.* **2021**, *11*, 35383–35391. [CrossRef]
40. Wang, L.; Berne, B.J.; Friesner, R.A. Ligand binding to protein-binding pockets with wet and dry regions. *Proc. Natl. Acad. Sci. USA* **2011**, *108*, 1326–1330. [CrossRef]
41. Matsunaga, A.; Saito, T. Impact of Apolipoprotein E Variants: A Review of Naturally Occurring Variants and Clinical Features. *J. Atheroscler. Thromb.* **2025**, *32*, 281–303. [CrossRef] [PubMed]
42. Kalidass, B.; Muthukaliannan, G.K. In silico profiling of phytochemicals for modulating amyloid beta–mediated immune regulation and neuroinflammation in Alzheimer's disease. *ACS Omega* **2025**, *11*, 14947–14963. [CrossRef]
43. Pantsar, T.; Poso, A. Binding Affinity via Docking: Fact and Fiction. *Molecules* **2018**, *23*, 1899. [CrossRef]
44. Nemergut, M.; Marques, S.M.; Uhrik, L.; Vanova, T.; Nezvedova, M.; Gadara, D.C.; Jha, D.; Tulis, J.; Novakova, V.; Planas-Iglesias, J.; et al. Domino-like effect of C112R mutation on ApoE4 aggregation and its reduction by Alzheimer's Disease drug candidate. *Mol. Neurodegener.* **2023**, *18*, 38. [CrossRef] [PubMed]
45. Dolai, S.; Pal, S.; Deepa, S.; Garai, K. Quantitative Assessment of Conformational Heterogeneity in Apolipoprotein E4 Using Hydrogen-Deuterium Exchange Mass Spectrometry. *J. Phys. Chem. B* **2024**, *128*, 10075–10085. [CrossRef] [PubMed]
46. Wang, C.; Najm, R.; Xu, Q.; Jeong, D.E.; Walker, D.; Balestra, M.E.; Yoon, S.Y.; Yuan, H.; Li, G.; Miller, Z.A.; et al. Gain of toxic apolipoprotein E4 effects in human iPSC-derived neurons is ameliorated by a small-molecule structure corrector. *Nat. Med.* **2018**, *24*, 647–657. [CrossRef]

47. Mahley, R.W.; Huang, Y. Small-molecule structure correctors target abnormal protein structure and function: Structure corrector rescue of apolipoprotein E4-associated neuropathology. *J. Med. Chem.* **2012**, *55*, 8997–9008. [CrossRef]
48. Patil, S.P.; Kuehn, B.R.; McCullough, C.; Bates, D.; Hazim, H.; Diallo, M.; Francois, N. Discovery of Isobavachin, a Natural Flavonoid, as an Apolipoprotein E4 (ApoE4) Structure Corrector for Alzheimer's Disease. *Molecules* **2025**, *30*, 940. [CrossRef]
49. Zhao, R.; Xiao, H.; Jin, T.; Xu, F.; Li, Y.; Li, H.; Zhang, Z.; Zhang, Y. Naringenin promotes cell autophagy to improve high-fat-diet-induced atherosclerosis in ApoE-/- mice. *Braz. J. Med. Biol. Res.* **2021**, *54*, e9764. [CrossRef]
50. Davra, V.; Benzeroual, K.E. Flavonoids and fibrate modulate apoE4-induced processing of amyloid precursor protein in neuroblastoma cells. *Front. Neurosci.* **2023**, *17*, 1245895. [CrossRef]
51. Stetefeld, J.; McKenna, S.A.; Patel, T.R. Dynamic light scattering: A practical guide and applications in biomedical sciences. *Biophys. Rev.* **2016**, *8*, 409–427. [CrossRef]
52. Facchinetti, R.; Valenza, M.; Bronzuoli, M.R.; Menegoni, G.; Ratano, P.; Steardo, L.; Campolongo, P.; Scuderi, C. Looking for a Treatment for the Early Stage of Alzheimer's Disease: Preclinical Evidence with Co-Ultramicronized Palmitoylethanolamide and Luteolin. *Int. J. Mol. Sci.* **2020**, *21*, 3802. [CrossRef]
53. Zhang, Z.; Sun, Z.; Jia, R.; Jiang, D.; Xu, Z.; Zhang, Y.; Wu, Y.Q.; Wang, X. Protective effects of polydatin against bone and joint disorders: The in vitro and in vivo evidence so far. *Nutr. Res. Rev.* **2024**, *37*, 96–107. [CrossRef] [PubMed]
54. Almeida, L.; Vaz-da-Silva, M.; Falcão, A.; Soares, E.; Costa, R.; Loureiro, A.I.; Fernandes-Lopes, C.; Rocha, J.F.; Nunes, T.; Wright, L.; et al. Pharmacokinetic and safety profile of trans-resveratrol in a rising multiple-dose study in healthy volunteers. *Mol. Nutr. Food Res.* **2009**, *53*, S7–S15. [CrossRef]
55. Wittemer, S.M.; Ploch, M.; Windeck, T.; Müller, S.C.; Drewelow, B.; Derendorf, H.; Veit, M. Bioavailability and pharmacokinetics of caffeoylquinic acids and flavonoids after oral administration of Artichoke leaf extracts in humans. *Phytomed. Int. J. Phytother. Phytopharm.* **2005**, *12*, 28–38. [CrossRef] [PubMed]
56. Beggiato, S.; Tomasini, M.C.; Ferraro, L. Palmitoylethanolamide (PEA) as a Potential Therapeutic Agent in Alzheimer's Disease. *Front. Pharmacol.* **2019**, *10*, 821. [CrossRef] [PubMed]